

A Precision Measurement of the W Boson Mass at $D\bar{O}$

Junjie Zhu

State University of New York at Stony Brook, Stony Brook, NY, 11794

(Dated: April 16, 2009)

I present the first measurement of the W boson mass in the electron decay channel using the Run II $D\bar{O}$ detector at the Fermilab Tevatron Collider. The data used was collected from 2002 to 2006 and the integrated luminosity is 1 fb^{-1} . The W boson mass was determined from the likelihood fit to the measured data distribution. The mass value is found to be $80.401 \pm 0.023(\text{stat}) \pm 0.037(\text{syst}) \text{ GeV} = 80.401 \pm 0.044 \text{ GeV}$ using the transverse mass spectrum, which is the most precise measurement from one single experiment to date. This result puts tighter constraints on the mass of the standard model Higgs boson. I also present three other measurements that can help to reduce the theoretical uncertainties for the future W mass measurements.

PACS numbers: 13.38.Be, 13.85.Qk, 14.60.Cd, 14.70.Fm

INTRODUCTION

The W and Z bosons are the gauge bosons that, along with the photon, mediate electroweak interactions. In the Standard Model (SM) of particle physics, the Higgs boson is introduced to break the electroweak symmetry and make W and Z bosons massive and photon massless. The W boson mass, m_W , can be written as

$$m_W = \sqrt{\frac{\pi\alpha}{\sqrt{2}G_F}} \times \frac{1}{\sin\theta_W\sqrt{1-\Delta r}} \quad (1)$$

where G_F is the Fermi constant, α is the electromagnetic coupling constant, θ_W is the weak mixing angle and has the relation $\cos\theta_W = m_W/m_Z$ in the “on-shell” scheme with m_Z as the mass of the Z boson [1]. Δr accounts for radiative corrections which are dominated by loop diagrams involving the top quark and the Higgs boson (see Fig 1).

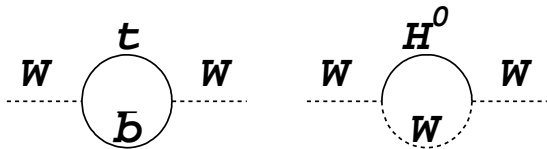


FIG. 1: Loop diagrams involving the top quark and the Higgs boson that contribute to the W boson mass.

Since m_Z , G_F and α have been measured very precisely, we can derive the size of the radiative corrections from the measured m_W . In the SM, the correction from the $t\bar{t}$ loop is proportional to m_t^2 , and the correction from the Higgs loop is proportional to $\ln m_H$ [2]. In extensions to the SM, new particles may give rise to additional corrections to the value of m_W . For example, in the minimal supersymmetric extension of the standard model (MSSM), additional corrections can increase the predicted m_W by up to 250 MeV [3]. A measurement of the W boson mass therefore constitutes a test of the SM, and a discrepancy with the SM prediction could indicate new physics.

Direct measurements of the W boson mass have been carried out at the CERN e^+e^- collider (LEP2) using W pair production and at the Fermilab $p\bar{p}$ collider (Tevatron) using the inclusive W boson production. The combined m_W value is $80.376 \pm 0.033 \text{ GeV}$ [4] from the LEP2 collider and $80.432 \pm 0.039 \text{ GeV}$ [5–7] from the Tevatron collider. The current world average value of the W boson mass is $80.399 \pm 0.025 \text{ GeV}$ [8].

To contribute equally to the uncertainty on the Higgs mass, the experimental uncertainties Δm_t and Δm_W have to satisfy $\Delta m_W \simeq 0.006 \times \Delta m_t$ [9]. The current combined Tevatron results on m_t have an uncertainty of 1.3 GeV, the equivalent Δm_W to get equal contribution to the Higgs mass uncertainty would be $\Delta m_W = 8 \text{ MeV}$, which is smaller than the current experimental error on m_W by more than a factor of three; the latter is therefore the limiting factor in precision tests and must be reduced.

In this paper, I present the single most precise measurement of the W boson mass using the data from the $D\bar{O}$ experiment [10]. In conjunction with the top quark mass measurement, the result shown in this paper leads to stricter bounds on the mass of the Higgs boson.

MEASUREMENT STRATEGY

In $p\bar{p}$ collisions, W and Z bosons are produced predominantly through quark-antiquark annihilation. Once they are produced, they will immediately decay to other leptons and quarks. We identify W and Z bosons by their leptonic decays. In this paper, only the electron decay channel $W \rightarrow e\nu$ is used due to the fine resolution of the calorimeter system at $D\bar{O}$. The decayed leptons (e and ν) typically have transverse momenta of about half the mass of the parent boson. The electron deposits its energy inside the electromagnetic calorimeter, and the neutrino escapes undetected. Due to the uninstrumented region at large rapidity, we can not reconstruct momenta for particles near the beam. Instead we have to use kinematic variables determined in the transverse plane perpendicular to the beam direction. For each W

(or Z) candidate, we observe in the calorimeter the electron(s) and the recoil system. The energy of the electron is measured by the EM calorimeter, and the direction is measured by the tracking system. The recoil system is determined using all energy in the calorimeter except that in the electron(s). Its transverse momentum vector, \vec{u}_T , is measured by summing the observed transverse energy flow vectorially over all calorimeter cells that are not associated with the reconstructed electron(s). Thus, we reduce the reconstruction of every candidate to a measurement of the momentum $\vec{p}(e)$ of the electron(s) and the transverse momentum \vec{u}_T of the recoil system. The missing transverse energy vector $\vec{\cancel{E}}_T$ can be calculated using $\vec{\cancel{E}}_T = -[\vec{p}_T(e) + \vec{u}_T]$, where $\vec{p}_T(e)$ is the transverse momentum vector of the electron. The characteristics for a $W \rightarrow e\nu$ candidate is shown in Fig. 2.

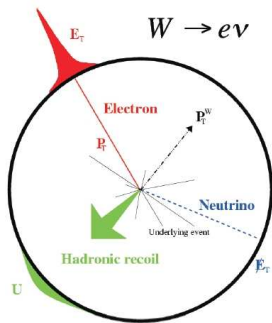


FIG. 2: $W \rightarrow e\nu$ event characteristics.

For each W candidate, three kinematic variables can be reconstructed: the transverse mass m_T , the electron transverse momentum p_T^e and the neutrino transverse momentum p_T^ν (inferred from $\vec{\cancel{E}}_T$). The transverse mass is calculated with the formula

$$m_T = \sqrt{2p_T^e p_T^\nu [1 - \cos(\phi_e - \phi_\nu)]}, \quad (2)$$

where ϕ_e and ϕ_ν are the azimuthal angles of the electron and neutrino respectively.

Because of the convolution of the boson production and decay with the detector response and resolution, the shapes of the three measured variables cannot be calculated analytically. Instead the measurement of m_W is obtained by a comparison of the spectra of the three different measurement variables with templates of the same variable distributions constructed from a parameterized Monte Carlo (MC) simulation with varying input W masses. $Z \rightarrow ee$ events are used for the tuning of many key aspects of the detector response to the electron and the recoil system in the MC simulation. Since we calibrate this response by forcing the observed di-electron mass peak in the $Z \rightarrow ee$ sample to agree with the known Z mass, we effectively measure the ratio of W and Z boson masses. Many systematic uncertainties on the W boson mass are reduced due to this fact.

The m_T and p_T^e measurements are complementary because the major cause of changes from the true to the measured spectrum for each quantity arises from different sources. The m_T variable has the advantage that its spectrum is relatively insensitive to the production dynamics of the W boson, but it is sensitive to the detector resolution. The p_T^e variable, on the other hand, is less sensitive to the detector resolution but more sensitive to the W production dynamics. Thus the two measurements have sensitivity to different components of the analysis.

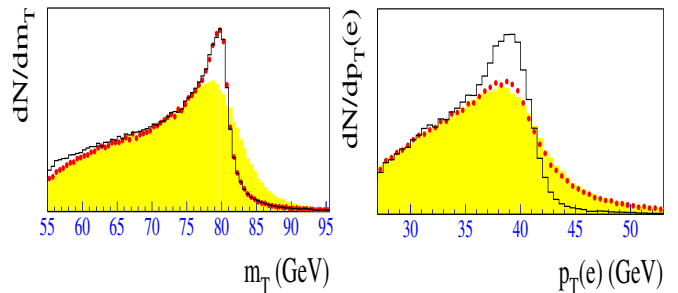


FIG. 3: The effects of resolution and the finite p_T^W on M_T (left) and $p_T(e)$ in $W \rightarrow e\nu$ events. The histogram shows the distribution without detector smearing and for $p_T^W = 0$. The dots include the effects of adding finite p_T^W , while the shaded histogram includes the effects of detector resolutions.

Since both the momentum of the electron $\vec{p}(e)$ and the transverse momentum of the recoil system \vec{u}_T are measured by the calorimeter, the calorimeter is the centerpiece of this measurement. To make a W boson mass measurement with an overall uncertainty of 50 MeV, it is necessary to achieve a measurement of the electron energy with a fractional uncertainty of 5×10^{-4} . It is therefore very important to calibrate the calorimeter and understand the response to high precision for this measurement.

DØ DETECTOR

The D0 detector [11] contains tracking, calorimeter and muon subdetector systems. Silicon microstrip tracking detectors (SMT) near the interaction point cover pseudorapidity $|\eta| < 3$ [12] to provide tracking and vertexing information. The central fiber tracker (CFT) surrounds the SMT, providing coverage to $|\eta| < 2.5$. A 2 T solenoid surrounds these tracking detectors.

Three uranium-liquid argon (LAr) calorimeters measure particle energies. The central calorimeter (CC) covers $|\eta| < 1.1$, and two end calorimeters (EC) extend coverage to $|\eta| < 4.2$. The CC is segmented in depth into eight layers. The first four layers are used primarily to measure the energy of photons and electrons and are collectively called the electromagnetic (EM) calorimeter. The remaining four layers, along with the first four, are

used to measure the energy of hadrons. Most layers are segmented into 0.1×0.1 regions in (η, ϕ) space. The third layer of the EM calorimeter is segmented into 0.05×0.05 regions. A cross sectional view of one quarter of the detector, showing the η and depth segmentation is shown in Fig. 4. In total, there are about 46,000 readout channels for the calorimeter system.

Muons are measured with stations which use scintillation counters and several layers of tracking chambers over the range $|\eta| < 2$.

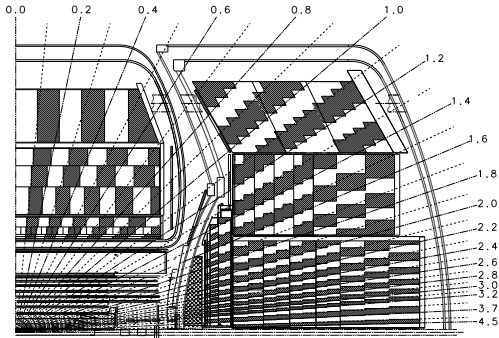


FIG. 4: Side-view of one quarter of the DØ calorimeter system, showing segmentation and tower definitions. The line extending from the center of the detector denote the pseudo-rapidity coverage of cells and projected towers.

EVENT SELECTION

The data used for this analysis were recorded in the period 2002-2006 and correspond to a total integrated luminosity of 1 fb^{-1} [13]. The data sample is initially defined by requiring candidate events to be recorded via a single-electron trigger. The primary vertex of the event must satisfy $|z_V| < 60 \text{ cm}$ where z_V is the primary vertex position along the beam line.

The requirements for the $W \rightarrow e\nu$ candidate are:

- one electron reconstructed in the fiducial region of the central calorimeter with $|\eta_{det}| < 1.05$ [12], passing electron shower shape and energy isolation requirements,
- one track matching the electron with a match probability $P > 0.01$, having at least one SMT hit and $p_T > 10 \text{ GeV}$,
- electron $p_T^e > 25 \text{ GeV}$,
- $\cancel{E}_T > 25 \text{ GeV}$,
- $u_T < 15 \text{ GeV}$ and
- $50 < m_T < 200 \text{ GeV}$.

The requirements for the $Z \rightarrow ee$ candidates are:

- two electrons satisfying the calorimeter and track match requirements described above. One electron must be reconstructed in the CC, and the other in either the CC or EC calorimeters,

- both electrons have $p_T^e > 25 \text{ GeV}$,
- $u_T < 15 \text{ GeV}$ and
- $70 < m_{ee} < 110 \text{ GeV}$,

in which m_{ee} is the invariant mass of the electron-positron pair.

These selections yield 499,830 candidate $W \rightarrow e\nu$ events and 18,725 candidate $Z \rightarrow ee$ events in which both electrons are in the central calorimeter.

PARAMETRIZED MC SIMULATION

The W boson mass is determined by comparisons between data and simulated m_T , p_T^e and \cancel{E}_T distributions.

The kinematics of W and Z boson production and decay are obtained from the RESBOS [14] and PHOTOS [15] programs. The RESBOS program uses a gluon resummation calculation at low boson p_T and perturbative QCD calculations at high boson p_T . The PHOTOS program is a universal MC program for final state radiation that can generate a maximum of two photons. Systematic uncertainty from radiation has been assessed by comparing the results from PHOTOS with those from WGRAD [16] and ZGRAD [17] which include initial state radiation (ISR) and interference effects. The CTEQ6.1M set of parton distribution functions (PDFs) and their uncertainties [18] are used.

The electron trigger efficiency, reconstruction efficiency, energy response and resolution are simulated using parametric functions and binned look-up tables. The response and resolution of the hadronic recoil is also simulated, again using a parametric model. These components of the simulation are described in the following two sub-sections.

I. ELECTRON SIMULATION

The electron selection efficiencies are modeled in the fast MC simulation by parameterizations derived using a combination of detailed GEANT simulation and data control samples. The purely electron-related trigger, reconstruction, identification and track efficiencies are derived from the $Z \rightarrow ee$ sample using the tag-and-probe method [19]. In most cases, the absolute efficiency has limited impact on the result, and only effects which distort the shapes of the m_T , p_T^e and \cancel{E}_T distributions impact this analysis. These efficiencies are parameterized as functions of η_e , p_T^e , and z_V where η_e is the electron pseudorapidity.

In addition to the electron-only effects, two other factors are important in determining the event-by-event efficiency. The first of these is the effect of additional hadronic energy in the calorimeter, typically arising from other $p\bar{p}$ interactions. This effect increases with increasing instantaneous luminosity because higher luminosity tends to increase the overall activity in the detector and thus reduce the electron selection efficiency. This effect

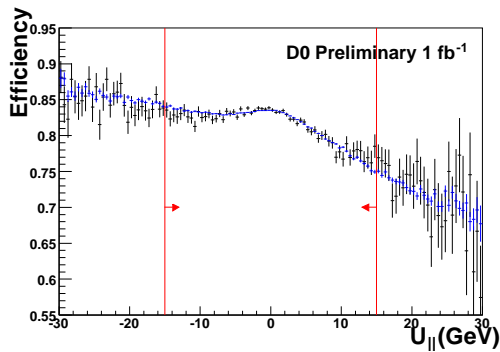


FIG. 5: The electron efficiency as a function of u_{\parallel} . The blue points are MC simulation results, and the black points are Z data. The regions outside the two red lines are not used in this analysis.

is parameterized using the event scalar E_T and p_T^e . The scalar E_T is the scalar sum of the transverse energies of all calorimeter cells outside the electron window. The control sample for parameterizing this effect is events simulated by the GEANT simulation with zero bias (ZB) events added to account for the instantaneous luminosity effects. ZB events are chosen by a trigger requiring only synchronization with the beam crossing clock.

The second factor occurs because of correlations in the W event topology. The electron selection efficiency depends on the relative orientation of the hadronic recoil and the electron. A variable called u_{\parallel} is introduced, which is the projection of the momentum of the recoil system along the electron direction. For negative values of u_{\parallel} (recoil system opposite to the electron), the electron is not affected by the recoil system and thus the electron selection efficiency is almost constant; for positive values of u_{\parallel} , the recoil system and the electron are on the same hemisphere, the electron selection efficiency decreases as u_{\parallel} increases. This u_{\parallel} efficiency is also determined using $Z \rightarrow ee$ events. Figure 5 shows the electron selection efficiency as a function of u_{\parallel} for data and fast MC simulation.

The relationship between the measured and true electron energy is given by

$$E = R_{EM}(E_0) \otimes \sigma_{EM}(E_0, \eta_e) + \Delta E(\mathcal{L}, u_{\parallel}) \quad (3)$$

where E_0 is the true electron energy, E is the reconstructed energy, $R_{EM}(E_0)$ is the response for a given E_0 , σ_{EM} is the energy resolution for EM objects and $\Delta E(\mathcal{L}, u_{\parallel})$ is a correction for energy included in the reconstructed electron energy which is not related to the electron energy deposition. This final correction is luminosity and topology dependent and is measured in $W \rightarrow e\nu$ data from the transverse energy observed in a region separated from the electron azimuthally.

The response of the EM calorimeter is modeled using

$$R_{EM}(E_0) = \alpha \times E_0 + \beta \quad (4)$$

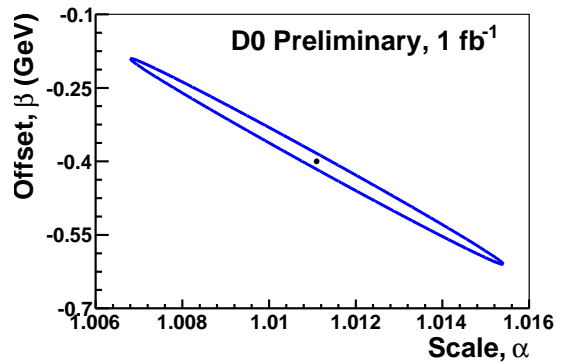


FIG. 6: The central value for α and β as determined from the fit to the Z mass distribution and the error ellipse defined by $\Delta\chi^2 = 1$.

where α is the response of the calorimeter to electrons and β is an offset. We determine α and β by fitting the Z mass distribution to that generated by the fast MC simulation for different α and β values. Figure 6 shows the central values and 1σ contour for α and β determined from the fit. The fitted values are

$$\begin{aligned} \alpha &= 1.0111 \pm 0.0043 \\ \beta &= -0.40 \pm 0.21 \text{ GeV} \end{aligned}$$

and the correlation is -0.997 . The uncertainty on m_W arising from the uncertainties on α and β is determined by varying the parameters by the 1σ contour including the correlation and propagating the effect to the final W mass.

The resolution of the EM calorimeter is modeled using

$$\frac{\sigma_{EM}(E, \eta)}{E} = \sqrt{C_{EM}^2 + \frac{S_{EM}^2}{E}} \quad (5)$$

where C_{EM} is the constant term and S_{EM} is the sampling term for the EM calorimeter. Because of the large amount of material in front of the calorimeter, S_{EM} is not constant, but depends on the electron energy and incident angle. The dependences were derived using the single energy electron events passed through the GEANT simulation.

The constant term was found using a fit of a Breit-Wigner line shape convoluted with a Gaussian to the Z peak. The Gaussian width characterizes the detector resolution. The value was derived by comparing the width of the Gaussian fitted to the Z peak predicted by the fast MC simulation and the data. The result from the fit is $C_{EM} = (2.04 \pm 0.13)\%$.

In addition, the need for a correction to account for different energy loss for electrons from W decay and those from Z decay was investigated. A difference could arise because W and Z electrons of the same energy have different pseudorapidity values and thus correspond to differences in material transversed. No need was found for

a correction with a precision of 4 MeV, which is applied as a systematic uncertainty.

II. RECOIL SYSTEM SIMULATION

The recoil, \vec{u}_T , is the vector sum of all transverse energy in the event not associated with the reconstructed electron. The recoil system mainly has two components: a hard component and a soft component.

The hard component essentially balances the transverse momentum of the vector boson. We use an ansatz function derived from $Z \rightarrow \nu\nu$ GEANT MC events to model the detector response to this component. The ansatz function depends on the generator level boson momentum and direction.

The soft component represents the other interactions such as underlying event and additional energy content in the event that contribute to the hadronic recoil. The underlying event energy is defined to be that from the interactions of the spectator partons of the same $p\bar{p}$ pair that produced the vector boson. This contribution is modeled using data minimum bias (MB) events with only one reconstructed primary vertex. MB events are chosen by a trigger requiring hits in both luminosity counters which are in time with a beam crossing. The additional energy content is associated with all the other interactions occurring in the $p\bar{p}$ pairs present in the same or previous beam crossings. Additional interactions are also included in this sub-component. It is modeled using data ZB events that have the same instantaneous luminosity profile as W boson candidates.

The recoil system also deposit energy inside the electron cluster window. That energy will be measured as part of the electron energy and needs to be subtracted from the recoil energy calculation. This correction is determined in W data events using distributions of energy measured in an equal sized window azimuthally separated from the electron and the hadronic recoil.

Some photons radiated from the electron or the W boson fall outside the electron reconstruction cone and hence are reconstructed as part of the recoil. Detailed simulation of the probability for the photons to reach the calorimeter and the response to these photons is also included in the fast MC simulation.

These four components above are derived using either detailed GEANT simulation or data events. Because the simulation alone is not expected to reproduce the true hard recoil with sufficient precision, the recoil model is then further tuned using data $Z \rightarrow ee$ events. The sum of the recoil \vec{u}_T and di-electron momentum \vec{p}_T^{ee} vectors in Z events is projected on to the $\hat{\eta}$ axis. The definition of $\hat{\eta}$ axis is shown in Fig. 7, and the $\hat{\eta}$ unit vector is the bisector of the two electron directions in the transverse plane in Z events [20]. The recoil model is then tuned using the imbalance of recoil and electron energy in the $\hat{\eta}$ projection, called η_{imb} . The η_{imb} mean is used to fine tune the recoil response, and the η_{imb} width is used to

fine tune the recoil resolution. By construction, the vector $\hat{\eta}$ is insensitive to the electron energy measurement. The tuning involves five parameters, and the parameters for the response and resolution were determined independently of each other. Figure 8 shows the mean and width of η_{imb} for data and the fast MC simulation as functions of p_T^{ee} . The χ^2/dof for the response fit is 3.1/7 and for the resolution fit is 4.5/8.

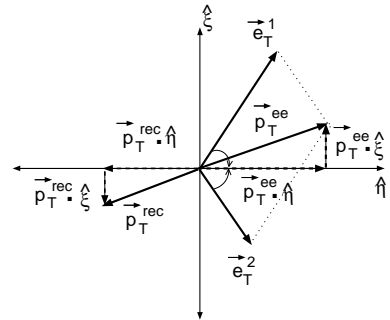


FIG. 7: Definition of the $\hat{\eta}$ axis for $Z \rightarrow ee$ events.

The systematic uncertainties arising from the recoil model are determined by propagating the uncertainties on the five tuning parameters derived from the fits.

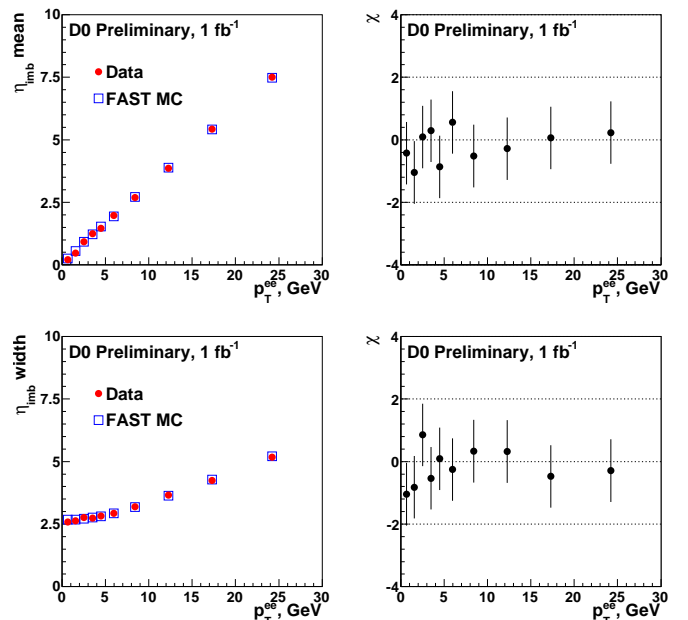


FIG. 8: The mean (upper left) and width (lower left) of η_{imb} as functions of p_T^{ee} and the χ values (right, upper and lower) for the difference between data and fast MC simulation are shown.

BACKGROUNDS

The backgrounds in the W sample are mainly $Z \rightarrow ee$ events in which one electron is not detected, QCD multi-jet events in which a jet is misidentified as an electron and \cancel{E}_T arises from misreconstruction, and $W \rightarrow \tau\nu \rightarrow e\nu\nu$ events. The three backgrounds are determined from either data or GEANT-based simulation [21]. The resulting backgrounds in terms of percent of the final sample are $(0.80 \pm 0.01)\%$ from $Z \rightarrow ee$, $(1.49 \pm 0.03)\%$ from QCD and $(1.60 \pm 0.02)\%$ from $W \rightarrow \tau\nu$.

RESULTS

The W mass is determined by fitting each of the data m_T , p_T^e and \cancel{E}_T distributions to corresponding distributions generated using the fast MC simulation. The MC templates are generated at a series of input W mass values with 10 MeV steps and backgrounds added to the simulated distributions. A binned likelihood between the data and template is then computed for each template. The resulting log likelihoods from each mass template are then fit to a parabola to determine the best fit W mass. The fits are performed separately for each of the m_T , p_T^e and \cancel{E}_T distributions.

The Z mass fit is shown in Fig. 9, the fitted Z mass is $91.185 \pm 0.033(\text{stat})$ GeV, agrees well with the world average value of 91.188 GeV. The W mass fit results from data are given in Table I.

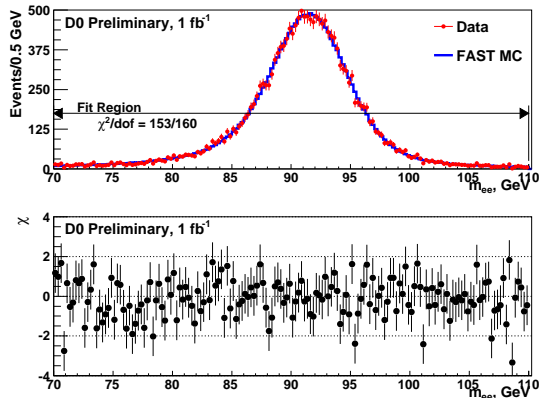


FIG. 9: The Z mass distribution in data and from the fast simulation (top) and the χ values for each bin (bottom). The χ value for a given bin is the difference between the data and the prediction divided by the statistical uncertainty from the data.

The distributions of each variable showing the data and MC template with backgrounds for the best fit value are shown in Fig. 10 through Fig. 12. These figures also show the bin-by-bin χ values defined as the difference between the data and template divided by the data uncertainty.

Variable	Fit Range (GeV)	Result (GeV)	χ^2/dof
m_T	$65 < m_T < 90$	80.401 ± 0.023	48/49
p_T^e	$32 < p_T^e < 48$	80.400 ± 0.027	39/31
\cancel{E}_T	$32 < \cancel{E}_T < 48$	80.402 ± 0.023	32/31

TABLE I: Results from the fits to data. The uncertainty is only the statistical component. The χ^2/dof values are computed over the fit range.

The systematic uncertainties in the W mass measurement arise from a variety of sources, but can roughly be categorized as those arising from experimental sources and those arising from theory. The methods used to derive the systematic uncertainties have been described in the corresponding sections above. The systematic uncertainties are summarized in Table II together with the statistical uncertainty.

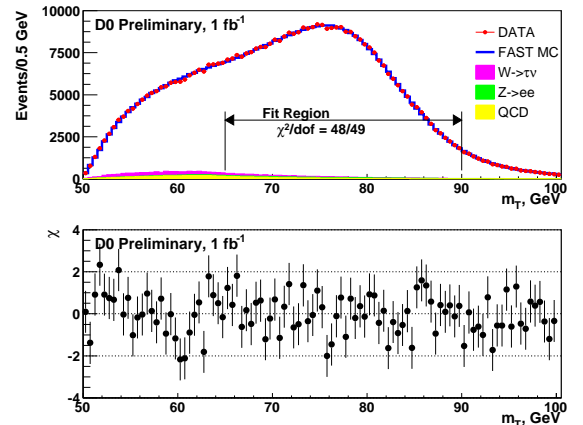


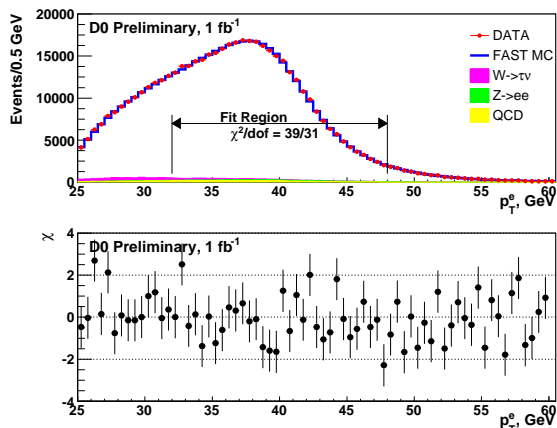
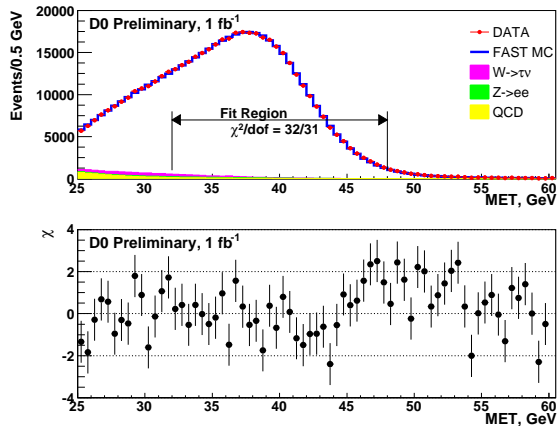
FIG. 10: The m_T distribution for data and fast MC simulation with backgrounds added (top), and the χ value for each bin (bottom).

OTHER MEASUREMENTS RELATED TO THE W BOSON MASS MEASUREMENT

The goal of the uncertainty on the W mass measurement from the Tevatron is 15 MeV [2]. For the measurement described here, the total experimental uncertainty is 35 MeV and the total theoretical uncertainty is 12 MeV using the m_T method. The experimental uncertainties are mainly limited by the statistical power of the $Z \rightarrow ee$ sample, and are expected to approximately scale as $1/\sqrt{N_Z}$ where N_Z is the number of Z events. Further reductions of the theoretical uncertainties are needed in order to reach the Run II goal.

The following describes other measurements that can help to reduce the theoretical uncertainties on the future m_W measurement:

Source	m_T (MeV)	p_T^e (MeV)	\cancel{E}_T (MeV)
Electron Energy Scale	34	34	34
Electron Energy Resolution	2	2	3
Electron Energy Nonlinearity	4	6	7
W/Z Electron Energy Loss Differences	4	4	4
Recoil Model	6	12	20
Electron Efficiencies	5	6	5
Backgrounds	2	5	4
PDF	9	11	14
QED	7	7	9
Boson p_T	2	5	2
Systematic Total	37	40	44
Statistical	23	27	23
Total	44	48	50

TABLE II: Systematic and statistical uncertainties on the W boson mass results.FIG. 11: The p_T^e distribution for data and fast MC simulation with backgrounds added (top), and the χ value for each bin (bottom).FIG. 12: The \cancel{E}_T distribution for data and fast MC simulation with backgrounds added (top), and the χ value for each bin (bottom).

I. W boson charge asymmetry measurement

The PDF uncertainty is currently the dominant source of the overall theoretical systematic uncertainty. The PDF uncertainty comes from the finite η coverage of the detectors, and increasing the electron acceptance would naturally reduce this uncertainty as demonstrated in Run I results [5]. Work is needed to realize increased acceptance. However, we can also make tighter constraints on PDFs using other Tevatron measurements. For example, the measurement of the W boson charge asymmetry is sensitive to the ratio of u to d quark densities in the proton and is of direct benefit in constraining PDF uncertainty in the W mass measurement. Fig. 13 shows the folded $W \rightarrow e\nu$ electron charge asymmetry as a function of η_e using 0.75 fb^{-1} of data [22]. The experimental uncertainties are smaller than the uncertainties due to PDFs for all except the last electron η bins. This measurement will improve the precision and accuracy of next generation PDF sets, and thus will help to reduce the PDF uncertainty on the W boson mass measurement.

II. Z/γ^* boson transverse momentum measurement

The underlying W boson p_T distribution is extracted from the measured Z boson p_T distribution using the ratio of the W and Z differential distributions obtained from theory. A detailed understanding of the Z boson p_T distribution is thus very important. For the W mass measurement mentioned here, only events with low p_T W and Z bosons are used due to the $u_T < 15 \text{ GeV}$ cut. For low p_T (approximately less than 30 GeV) bosons, the emission of multiple soft gluons dominates the QCD corrections to the cross section, and a soft gluon resummation technique was developed by Collins, Soper, and Sterman [24] to give reliable predictions. The CSS resummation formalism allows the inclusion of contributions from all soft gluons in an effective resummed form factor. The parameters used in the effective resummed form factor have to be derived from the experimental data. The un-

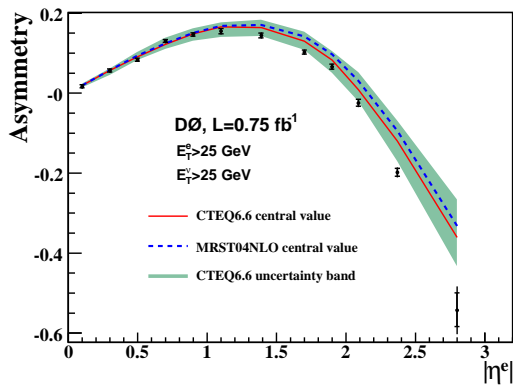


FIG. 13: The folded electron charge asymmetry distribution. The horizontal bars show the statistical uncertainty and the full vertical lines show the total uncertainty on each point. The solid (dashed) line is the theoretical prediction for the asymmetry using the CTEQ6.6 (MRST04NLO [23]) central PDF set. The shaded band is the uncertainty band determined using the 44 CTEQ6.6 PDF uncertainty sets.

certainty due to these parameters was found to be small (< 5 MeV). However, recent studies of data from deep inelastic scattering (DIS) experiments [25] indicate that the resummed form factor used for the inclusive Z/γ^* production may need to be modified for processes involving a small- x parton in the initial state. Ref. [26] indicates how such a modification would influence the p_T distributions of vector and Higgs bosons produced in hadronic collisions. A wider transverse momentum distribution is predicted for Z bosons with large rapidity (called “small- x broadening”). Besides the measurement of the normalized differential cross section as a function of Z/γ^* p_T , we also performed the first test of the small- x predictions using Z/γ^* bosons with $|y| > 2$ [27]. Our data disfavor the predictions with the small- x effect included, as shown in Fig. 14.

III. Z/γ^* boson forward-backward asymmetry and indirect determination of the W boson mass

The understanding of QED radiative correction is also crucial for a high precision W mass measurement. A large contribution to this uncertainty is the effect of electroweak corrections (FSR, ISR and interference terms). The forward-backward charge asymmetry (A_{FB}) distribution in $Z/\gamma^* \rightarrow ee$ events can be used to extract the effective weak mixing angle ($\sin^2 \theta_W$). $\sin^2 \theta_W$ is sensitive to the electroweak corrections [28]. Fig. 15 shows the comparison between the unfolded A_{FB} and two theoretical predictions using the PYTHIA [29] and ZGRAD [17] program. With the measured $\sin^2 \theta_W$ value 0.2326 ± 0.0019 , and the relation $\sin^2 \theta_W = 1 - m_W^2/m_Z^2$ in the “on-shell” scheme, an indirect measurement of the W boson mass is found to be 80.318 ± 0.100 GeV.

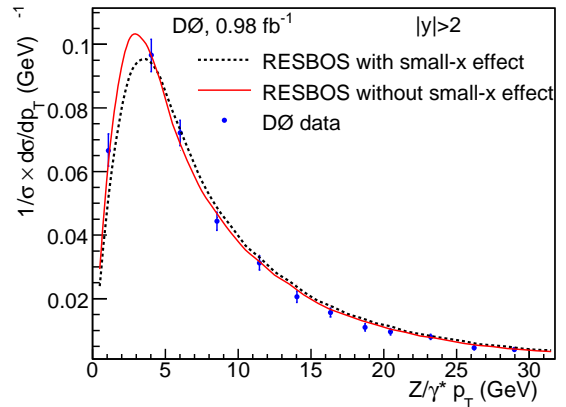


FIG. 14: The normalized differential cross section as a function of p_T for Z/γ^* boson with rapidity $|y| > 2$ and $p_T < 30$ GeV. The points are the data, the solid curve is the RESBOS prediction, and the dashed line is the prediction from the form factor modified after studies of small- x DIS data.

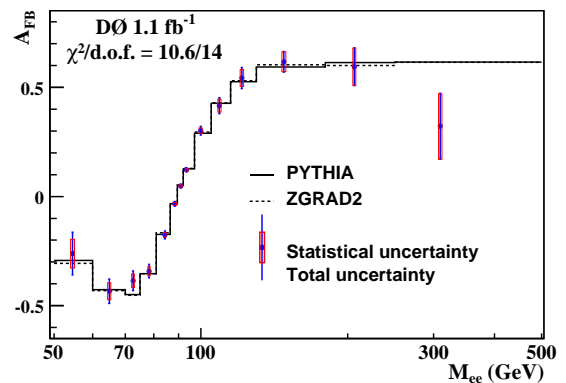


FIG. 15: Comparison between the unfolded A_{FB} (points) and the PYTHIA (solid curve) and ZGRAD2 (dashed line) predictions. The inner (outer) lines show the statistical (total) uncertainty.

CONCLUSIONS

I present the W boson mass measurement using the $W \rightarrow e\nu$ mode and 1 fb^{-1} of $DØ$ data. The mass measured using three different kinematic variables has been found to be 80.401 ± 0.044 GeV using m_T spectrum, 80.400 ± 0.048 GeV using p_T^e spectrum, and 80.402 ± 0.050 GeV using \cancel{E}_T spectrum. Figure 16 shows this result together with results from previous measurements. The result shown here is in good agreement with other measurements and is the most precise measurement from one single experiment. By including our result, the combined uncertainty from the Tevatron collider is smaller than the combined uncertainty from the LEP collider for the first time. This result will put tighter constraints on the mass of the Higgs boson. I also present three other measurements that can help to reduce the theoretical uncertainties for the future W boson mass measurements.

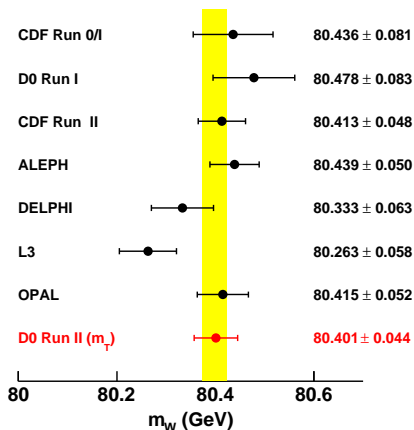


FIG. 16: Comparison of this measurement with all previously published measurements. This result is the most precise W boson mass measurement from one single experiment to date.

ACKNOWLEDGMENTS

I thank my $D\bar{O}$ colleagues and everyone who provided their help for this writeup. This work was supported by DOE Grant DEFG0292ER40697.

The material presented here is based on the following papers that I have made important contributions:

- *Measurement of the W boson mass at $D\bar{O}$* , to be submitted to Phys. Rev. Lett. [10]
- *Measurement of W boson charge asymmetry in electron channel*, Phys. Rev. Lett. **101**, 211801 (2008).
- *Measurement of the forward-backward asymmetry and extraction of $\sin^2\theta_W^{eff}$ in $p\bar{p} \rightarrow Z/\gamma^* \rightarrow ee$ events produced at $\sqrt{s} = 1.96$ TeV*, Phys. Rev. Lett. **101**, 191801 (2008).
- *Measurement of the shape of the boson transverse momentum distribution in $p\bar{p} \rightarrow Z/\gamma^* \rightarrow ee$ events produced at $\sqrt{s} = 1.96$ TeV*, Phys. Rev. Lett. **100**, 102002 (2008).

-
- [1] A. Sirlin, Phys. Rev. D **22**, 971 (1980).
 [2] D. Glenzinski and U. Heintz, Annu. Rev. Nucl. Part. Sci. **50**, 207 (2000); A. Kotwal and J. Stark, Annu. Rev. Nucl. Part. Sci. **58**, 147 (2008).
 [3] P. Chankowski *et al.*, Nucl. Phys. **B417**, 101 (1994); D. Garcia and J. Sola, Mod. Phys. Lett. A **9**, 211 (1994); D. Pierce *et al.*, Nucl. Phys. **B491**, 3 (1997).
 [4] S. Schael *et al.* (ALEPH Collaboration), Eur. Phys. J. C **47**, 309 (2006); J. Abdallah *et al.* (DELPHI Collaboration), Eur. Phys. J. C **55**, 1 (2008); arXiv:0803.2534v1

- [Eur. Phys. J. C (to be published)]; P. Achard *et al.* (L3 Collaboration), Eur. Phys. J. C **45**, 569 (2006); G. Abbiendi *et al.* (OPAL Collaboration), Eur. Phys. J. C **45**, 307 (2006).
 [5] V. M. Abazov *et al.* (D0 Collaboration), Phys. Rev. D **66**, 012001 (2002); B. Abbott *et al.* (D0 Collaboration), Phys. Rev. D **58**, 092003 (1998); B. Abbott *et al.* (D0 Collaboration), Phys. Rev. D **62**, 092006 (2000).
 [6] T. Affolder *et al.* (CDF Collaboration), Phys. Rev. D **64**, 052001 (2001).
 [7] T. Aaltonen *et al.* (CDF Collaboration), Phys. Rev. Lett. **99**, 151801 (2007); T. Aaltonen *et al.* (CDF Collaboration), Phys. Rev. D **77**, 112001 (2008).
 [8] The LEP ElectroWeak Working Group, CERN-PH-EP/2008-20; arXiv:0811.4682 [hep-ex] (2008).
 [9] M. Awramik *et al.*, Phys. Rev. D **69**, 053006 (2004).
 [10] V.M. Abazov *et al.* (D0 Collaboration), <http://www-d0.fnal.gov/Run2Physics/WWW/results/prelim/EW/E27>.
 [11] V.M. Abazov *et al.* (D0 Collaboration), Nucl. Instrum. Methods Phys. Res. A **565**, 463 (2006).
 [12] D0 uses a cylindrical coordinate system with the z axis running along the beam axis in the proton direction. Angles θ and ϕ are the polar and azimuthal angles, respectively. Pseudorapidity is defined as $\eta = -\ln[\tan(\theta/2)]$ where θ is measured with respect to the interaction vertex. In the massless limit, η is equivalent to the rapidity $y = (1/2)\ln[(E+p_z)/(E-p_z)]$. η_{det} is the pseudorapidity measured with respect to the center of the detector.
 [13] T. Andeen *et al.*, FERMILAB-TM-2365 (2007).
 [14] C. Balazs and C.P. Yuan, Phys. Rev. D **56**, 5558 (1997).
 [15] E. Barbiero and Z. Was, Comp. Phys. Commun. **79**, 291 (1994).
 [16] U. Baur, S. Keller and D. Wackerth, Phys. Rev. D **59** 013002 (1999).
 [17] U. Baur, S. Keller and D. Wackerth, code available at <http://ubhex.physics.buffalo.edu/~baur/zgrad2.tar.gz>
 [18] H.L. Lai *et al.*, Phys. Rev. D **55**, 1280 (1997); J. Pumplin *et al.*, JHEP **0310**, 046 (2003);
 [19] V. M. Abazov *et al.* (D0 Collaboration), Phys. Rev. D **76**, 012003 (2007).
 [20] J. Alitti *et al.* (UA2 Collaboration), Phys. Lett. B **276**, 354 (1992).
 [21] R. Brun and F. Carminati, CERN Program Library Long Writeup W5013 (1993).
 [22] V. M. Abazov *et al.* (D0 Collaboration), Phys. Rev. Lett. **101**, 211801 (2008).
 [23] A. D. Martin, R. G. Roberts, W. J. Stirling, and R. S. Thorne, Phys. Lett. B **604**, 61 (2004).
 [24] J. Collins, D. Soper, and G. Sterman, Nucl. Phys. **B250**, 199 (1985).
 [25] P. Nadolsky, D.R. Stump, and C.P. Yuan, Phys. Rev. D **61**, 014003 (2000); Phys. Rev. D **64**, 114011 (2001).
 [26] S. Berge *et al.*, Phys. Rev. D **72**, 033015 (2005).
 [27] V. M. Abazov *et al.* (D0 Collaboration), Phys. Rev. Lett. **100**, 102002 (2008).
 [28] V. M. Abazov *et al.* (D0 Collaboration), Phys. Rev. Lett. **101**, 191801 (2008).
 [29] T. Sjöstrand *et al.*, Comput. Phys. Commun. **135**, 238 (2001).